SCIENCE CHINA
Earth Sciences

•ARTICLE•

https://doi.org/10.1007/s11430-024-1690-7

El Niño-Southern Oscillation induced migration of typhoon tracks in the northwestern Pacific Ocean over the last two millennia

Shuo ZHANG[1,2], Vittorio MASELLI[3], Zhenyu ZHANG[2], Yang YANG[4], Xiaolin WANG[5], Xing JIAN[6], Yong SHI[2] & Jianhua GAO[2*]

[1] *Key Laboratory of Marine Geology and Environment, Institute of Oceanology, Chinese Academy of Sciences, Qingdao 266071, China*
[2] *Key Laboratory of Coast and Island Development of the Ministry of Education, School of Geography and Ocean Science, Nanjing University, Nanjing 210023, China*
[3] *Department of Chemical and Geological Sciences, University of Modena and Reggio Emilia, Modena 41100, Italy*
[4] *College of Marine Science and Engineering, Nanjing Normal University, Nanjing 210023, China*
[5] *State Key Laboratory of Critical Earth Material Cycling and Mineral Deposits, School of Earth Sciences and Engineering, Nanjing University, Nanjing 210023, China*
[6] *State Key Laboratory of Marine Environmental Science, College of Ocean and Earth Sciences, Xiamen University, Xiamen 361102, China*

Received September 11, 2024; revised September 3, 2025; accepted September 8, 2025; published online October 20, 2025

Abstract Revealing the spatiotemporal relationship between typhoon variability and climate conditions, and accurately predicting typhoon activities, is crucial for improving hazard scenarios in coastal regions. However, the short meteorological record restricts a comprehensive understanding of typhoon variation driven by climate change, necessitating the reconstruction of paleo-typhoons through geological records. In this study, two sediment cores from the East China Sea inner shelf muddy belt, northwestern Pacific, were analyzed to reconstruct the paleo-typhoons quantitatively over the last ~2000 yr. Our results revealed two periods of increased typhoon activity, namely ~1.6 to 1.1 ka, and ~0.5 to 0 ka, which were consistent with La Niña-dominated intervals. Meanwhile, in the East China Sea inner shelf muddy belt, the proportion of silt sediments from Taiwan, whose transport process is dominated by typhoon activities, significantly increased. During La Niña-dominated intervals, the relatively cold Indo-Pacific Warm Pool induced a southwestward migration of typhoons by driving the westward migration of the rising limb of the Walker Circulation and the equatorward contraction of the Hadley Cell. Consequently, more typhoons made landfall in southeast China during La Niña-dominated intervals. In addition, the peak maximum typhoon frequency in southeast China during the Little Ice Age was a consequence of the combined effects of La Niña-like intervals and the contraction and migration of the intertropical convergence zone. Our findings emphasized the force of El Niño-Southern Oscillation phase oscillation on typhoon tracks in the northwestern Pacific over several centuries, and the relative proportion of Taiwan sediments in the shelf muddy belt can reflect the changes in typhoon frequency over longer timescales. These results contribute valuable insights for paleoclimatic, paleoenvironmental, and sedimentological studies in East Asia during the Holocene.

Keywords Paleo-typhoon reconstruction, Northwestern Pacific, El Niño-Southern Oscillation, Raman spectroscopy, East China Sea

Citation: Zhang S, Maselli V, Zhang Z, Yang Y, Wang X, Jian X, Shi Y, Gao J. 2025. El Niño-Southern Oscillation induced migration of typhoon tracks in the northwestern Pacific Ocean over the last two millennia. Science China Earth Sciences, 68, https://doi.org/10.1007/s11430-024-1690-7

* Corresponding author (email: jhgao@nju.edu.cn)

1. Introduction

Tropical cyclones (referred to as typhoons in the northwestern Pacific and hurricanes in the North Atlantic) are among the costliest disasters affecting coastal regions (Zhou et al., 2019). Their frequency, intensity, and paths are determined by climatic conditions (Wang and Chan, 2002; Elsner and Liu, 2003; Studholme et al., 2022). Meteorological records and model results show that global warming has caused a decrease in the frequency of global tropical cyclones, but has significantly increased their intensity (Webster et al., 2005; Mei et al., 2015). These trends have either been attributed to global warming (Emanuel, 2005; Sobel et al., 2016) or to the interdecadal cyclical change of typhoons (Goldenberg et al., 2001; Chan, 2006).

The northwestern Pacific is globally the most active area for tropical cyclones (Bramante et al., 2020). Meteorological data from the past few decades have revealed that typhoon characteristics in this region are influenced by climate variation and oscillations in the ocean-atmosphere system (Chan, 2006; Camargo et al., 2007). However, significant uncertainties have been observed in the long-term relationship between climate conditions and typhoon activity. To expand this time window, geological records have been investigated to understand typhoon activity during the Holocene (Woodruff et al., 2009; Yu et al., 2009; Chen et al., 2012; Zhou et al., 2019; Bramante et al., 2020; Yang et al., 2020a, 2022). Compared to the North Atlantic (Yang et al., 2020b and references therein), pre-modern reconstructions of typhoon activities in the northwestern Pacific are sparse. Additionally, the various indicators (e.g., coarse content and Sr concentration in sediment) used in paleo-typhoon reconstruction vary in their sensitivities, complicating the comprehensive comparison of typhoons within the ocean basin and often making the findings and subsequent interpretations inconsistent. Therefore, quantitative reconstructions of paleo-typhoon activities are necessary in the northwestern Pacific for basin-scale comparison and global teleconnection of tropical cyclones.

The southeastern margin of Chinese mainland is significantly influenced by typhoons with straight tracks (Elsner and Liu, 2003, Figure 1b), implying that the typhoon frequency in southeast China is sensitive to the migration of typhoon tracks and typhoon numbers. The muddy belt in the East China Sea inner shelf, dominated by silt to clay, receives coarse sediment only during typhoon events, suggesting a potential for recording paleo-typhoons (Zhou et al., 2019). Major climate fluctuations during the late Holocene (last 2000 yr) include the Roman Warm Period, the Dark Ages Cold Period (DACP), the Medieval Warm Period (MWP), the Little Ice Age (LIA), and the 20th-century warm period (Yan et al., 2011). Furthermore, the hydroclimatic factors—Sea surface temperature (SST) of the Indo-Pacific Warm Pool (IPWP), the El Niño-Southern Oscillation (ENSO) phases, and the strength and position of the intertropical convergence zone (ITCZ)—oscillated periodically (Haug et al., 2001; Oppo et al., 2009; Yan et al., 2011; Denniston et al., 2016). These variations may cause changes in the numbers and (or) migration of typhoon genesis and tracks in the northwestern Pacific. Therefore, studying the geological record of the last two millennia is crucial to understanding the typhoon variation dynamics.

Two sediment cores (C07 and C10) from the southern part of the East China Sea muddy belt were used to investigate the typhoon activities in southeast China since ~2 ka, and sediments from the potential source regions of these two cores were analyzed (Figure 1c). Grain size analyses on coarse fractions, combined with a novel approach based on Raman spectroscopy to identify petrogenic organic carbon from the fine-grained fractions, were used to quantify the typhoon activities in the East China Sea over the last ~2000 yr. This was followed by a comparison of the existing paleo-typhoon records in the northwestern Pacific and paleo-hydroclimate proxies to reconstruct typhoon tracks and identify possible mechanisms driving the observed changes.

2. Geological setting

The inner shelf of the East China Sea receives large amounts of fluvial sediments from the Yangtze River (480 Mt yr^{-1}) and Taiwan rivers (50 to 150 Mt yr^{-1}) . The Yangtze River-sourced sediment formed a muddy belt along the inner shelf over the last ~7,000 yr, while the Taiwan fine sediments are discharged into the southern part of the muddy belt (Zhang et al., 2022a). Additionally, the rivers in southeast China discharge sand to the muddy belt, with a relatively low flux of <10 Mt yr^{-1} (Liu et al., 2018).

Typhoons in the northwestern Pacific could be divided into three groups based on their tracks (Elsner and Liu, 2003); the study area is dominated by straight-moving typhoons (Figure 1b). Typhoons significantly influence sediment discharge, particularly in the southern portion of the muddy belt. Typhoon-driven precipitation accounts for ~70% and ~75% of the drainage annual precipitation of the Minjiang (the largest river in southeast China) and Choshui (the largest river in Taiwan) Rivers, respectively (Figure 1d). For instance, during the typhoon "Mindulle" in 2004, the Choshui River discharged ~70 Mt of sediment, with the finer fraction (<63 μm) being transported by Taiwan warm currents and deposited in the southern muddy belt (Milliman et al., 2007). The sediment discharged by the Minjiang River is composed of sand and usually deposits within the estuary (Wang et al., 2020). During typhoon events, tongue-shaped suspended sand extends from the Minjiang River mouth to the southern muddy belt (Li et al., 2018).

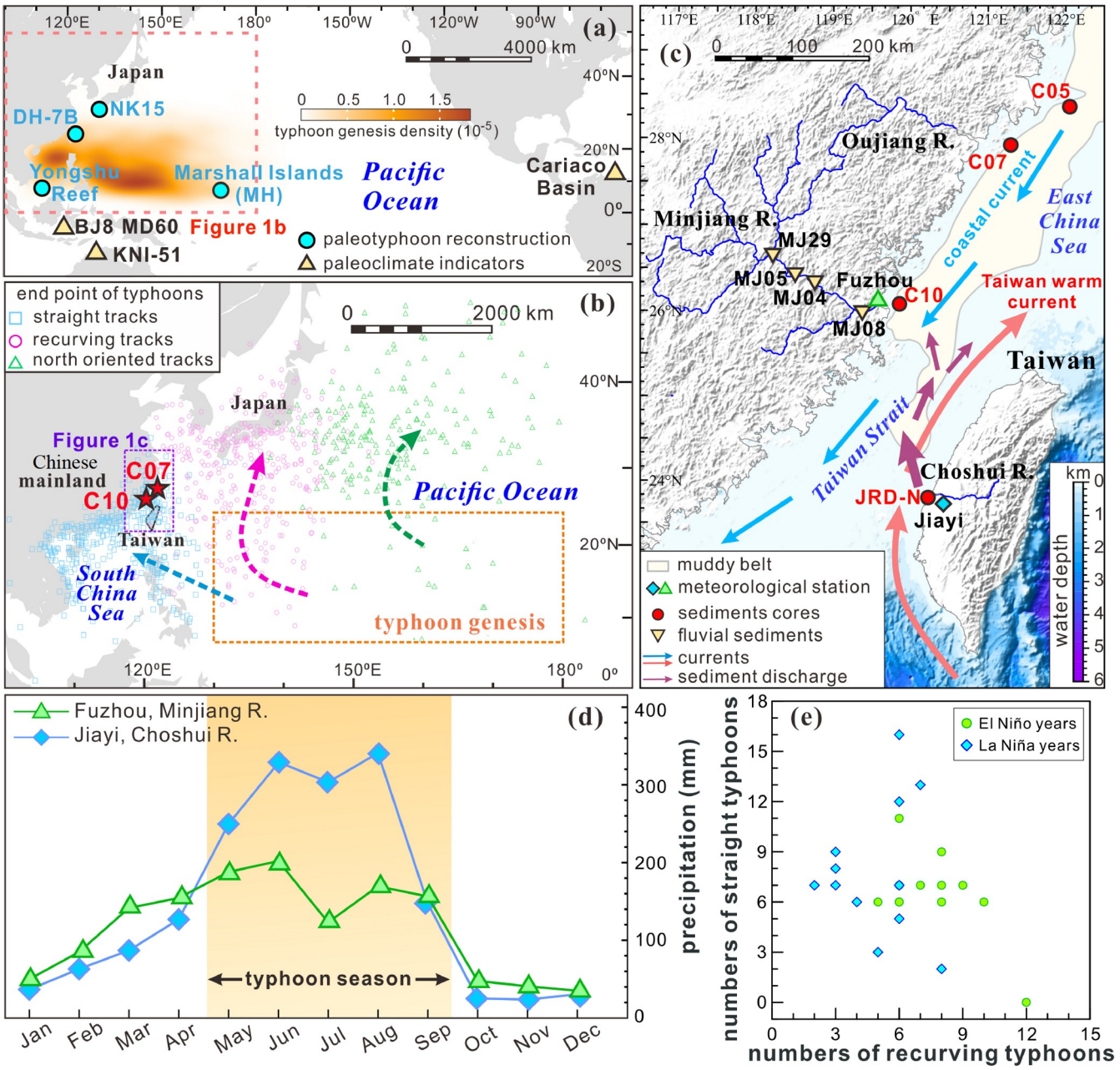

Figure 1 Geological and climatic background of the study region. (a) Typhoon genesis density and sample location in previous studies; (b) average tracks (dotted arrow) and end points of typhoons with different tracks (Elsner and Liu, 2003); (c) sample location in this study; (d) monthly precipitation in Jiayi, Taiwan, and Fuzhou, southeast China, location was shown in Figure 1c; (e) the number of recurving and straight typhoons during the ENSO years, the typhoon data followed Elsner and Liu (2003), and the ENSO phases followed Camargo et al. (2007).

3. Sampling and methods

3.1 Analysis methods

Sediment cores C07 (121°42.19′E, 27°45.80′N, water depth: 40 m, length: 515 cm) and C10 (119°52.21′E, 25°50.00′N, water depth: 25 m, length: 530 cm) from the southern muddy belt in the East China Sea were analyzed using a multi-proxy approach for paleo-typhoon reconstruction. Additionally, sediments from potential source regions of the southern muddy belt, including four fluvial sediments from the Minjiang River basin, core C05 from the northern muddy belt, and core JRD-N from the delta of the Choshui River, Taiwan, were also analyzed for provenance investigation (location in Figure 1c and detailed information in Tables S1 and S2 in supporting information).

Age models for cores C07 and C10 were reconstructed using Accelerator Mass Spectrometer ^{14}C dating of planktonic foraminifera, and the results were rectified by a Bayesian model (Blaauw and Christen, 2011, Figure 2a and 2b, Table 1). Additionally, 15 samples in the interval of

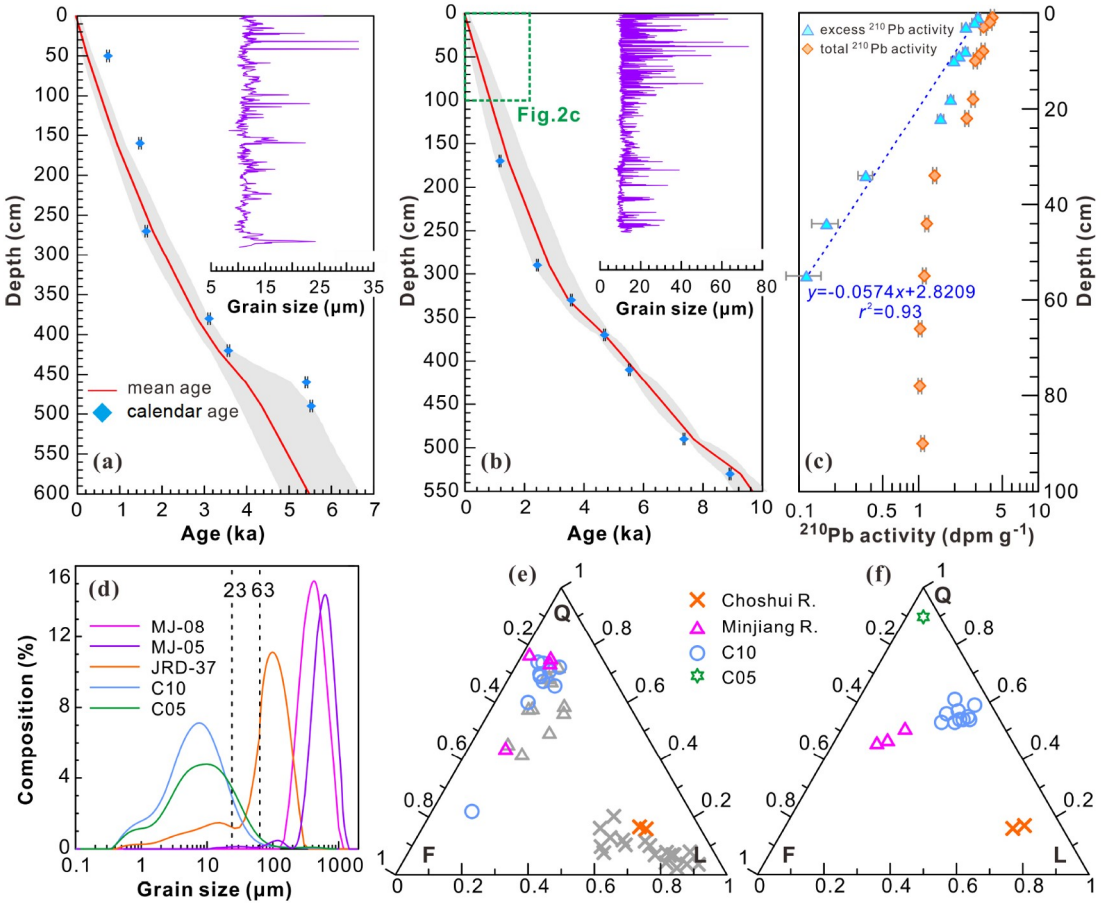

Figure 2 Chronological and provenance information of the sediment. Calendar age-depth model and mean grain size in (a) core C07 and (b) core C10; (c) ^{210}Pb dating in core C10; (d) grain size composition, the grain size of cores C05 and C10 represents the mean values from sediment with ages <2 ka; the relative proportion of quartz (Q), feldspar (F), and lithic fragment (L) in the (e) fraction with 63–500 μm and (f) fraction with 23–63 μm, gray symbols are data from Jian et al. (2020) and Zhang et al. (2022b).

1–90 cm for C10 were selected for ^{210}Pb dating (Figure 2c), following the method of Goldburg and Koide (1963). Grain size in the top 292 cm of core C07 (with 0.5 cm resolution) and the top 255 cm of core C10 (with 0.25 cm resolution) were analyzed to reconstruct paleo-typhoon activity (Figure 2a and 2b). The 63–500 μm and 23–63 μm fractions of 17 samples from core C05, C10, JRD-N, and fluvial sediments were selected for mineralogy analysis to determine the sediment provenance. Eleven samples from cores C05, C10, and JRD-N were selected for metamorphic peak temperature (MPT) analysis using Raman spectroscopy of petrogenic organic carbon for the <63 μm fraction to investigate the proportion of typhoon-induced fine sediments (Test S1 in supporting information for experimental procedures).

3.2 Reconstruction of paleo-typhoons based on coarse fraction

A simple statistical analysis of sediment grain size in cores C07 and C10 was conducted, following Donnelly et al. (2015) and Bramante et al. (2020), to identify the event threshold. First, the coarse fraction anomaly for cores C07 and C10 was calculated by subtracting a 10-point moving average from the coarse fraction data that excludes coarse fraction values >10% (Figure 3a and 3b). The higher magnitude coarse fraction peaks may exert a large influence on the filter and cause the adjacent smaller peaks to be ignored (Donnelly et al., 2015). This filter limits the influence of intergenerational variations in local background deposition processes while preserving coarse fraction peaks that may be associated with short-duration storm events (Bramante et al., 2020). Events were then defined as coarse anomaly peaks that exceeded 1.0 standard deviations (Donnelly et al., 2015). Once all events were identified (Figure 3a and 3b), we calculated the event frequency per 100 yr following Lane et al. (2011).

3.3 Provenance analysis of fine fraction based on the MPT of petrogenic organic carbon

Considering that typhoon events play key roles in fine fluvial sediment transport from Taiwan to the muddy belt (Milliman

Table 1 The ^{14}C age and calendar age of cores C07 and C10

Core	Depth (cm)	^{14}C age (a)	Error (a)	Calendar age (cal. yr BP)
C07	50	770	30	725
	160	1620	30	1481
	270	1740	30	1629
	380	2950	30	3111
	420	3345	30	3567
	460	4635	30	5411
	490	4760	30	5525
C10	170	1780	30	1177
	290	2850	30	2432
	330	3800	30	3572
	370	4655	30	4690
	410	5350	30	5524
	490	7050	30	7360
	530	8500	30	8910

et al., 2007), the proportion of Taiwan-sourced fine sediment in the muddy belt could imply the typhoon activities in southeast China over a long timescale. Raman spectrum can quantitatively reveal the MPT of petrogenic organic carbon with a range of 330–640°C or even lower temperatures (Beyssac et al., 2002; Lahfid et al., 2010). This technique is useful for provenance analysis when the metamorphic rocks in potential source areas exhibit distinct differences (Jiao et al., 2018; Sparkes et al., 2020). The MPT of carbon was calculated from Raman spectral analysis using eqs. (1) to (4) of Beyssac et al. (2002) and Lahfid et al. (2010).

$$R2 = D1 / (G + D1 + D2)_{\text{area}}, \quad (1)$$

$$RA2 = (D1 + D4) / (G + D2 + D3)_{\text{area}}, \quad (2)$$

$$T_{R2} = -445 \times R2 + 641, \quad (3)$$

$$T_{RA2} = (RA2 - 0.27) / 0.0045, \quad (4)$$

where T_{R2} and T_{RA2} mean MPT, appropriate for organic carbon with MPT <330 and >330°C, respectively; G, $D1$, $D2$, $D3$, and $D4$ are characteristic peaks of carbon at 1580, 1350, 1620, 1500 cm^{-1}, and 1150 to 1250 cm^{-1} in Raman spectrums, respectively (Figure 4a); $R2$ and $RA2$ are parameters calculated based on the peak area of the characteristic peaks. All data were obtained from the Raman spectra using the Origin 2017 program.

This was followed by the calculation of the sediment contribution ratio for core C10, considering cores C05 and JRD-N as the two main provenance sources. The provenance of JRD-N has remained relatively stable since ~11 ka (Zhang et al., 2022b). Therefore, the sample JRD-38, with an age of ~1.0 ka, can be considered representative for the provenance information of core JRD-N during 2.0 to 0 ka. However, the ε_{Nd} values in core C05 exhibited significant variability, indicating changes in provenance over the last 2 millennia (Zhang et al., 2023). To minimize the influence of provenance changes in core C05 on our results, we selected isochronous samples from C05 to calculate the sediment proportion in C10 (Figure 4). The calculation method is referred to eqs. (5) and (6).

$$CDF_{C10} = P_{C05} \times CDF_{C05} + P_{C10} \times CDF_{C10} P_{JRD\text{-}N} \times CDF_{JRD\text{-}N}, \quad (5)$$

$$P_{C05} + P_{C10} = 1, \quad (6)$$

where the CDF is the cumulative distribution function of MPT in sediment samples, P is the sediment contribution ratio of C05 and JRD-N in core C10, calculated by the method proposed in Jiao et al. (2018). The CDF was modeled by a Markov Chain Monte Carlo method, which was finished in a Matlab implementation (Figure 4h–4l).

4. Results

4.1 Lithology and chronology

The sediments with age <2.1 ka in cores C07 and C10 consist of homogeneous gray to dark gray clay silt, showing no significant disturbances. Sediments of core C07 and C10 are predominantly composed of silt, with average proportions of 83.2% and 82.6%, respectively. The sand content varies from 0 to 8% in core C07 (average = 0.8%), and from 0 to 21.8% in core C10 (average = 1.5%). The ^{14}C dating of the cores revealed relatively stable and high deposition rates over the last two millennia, ranging from 0.07 to 0.12 cm yr^{-1} in core C07, and 0.10 to 0.14 cm yr^{-1} in core C10. The continuous lithology and relatively stable deposition rates suggest a consistent sedimentary environment. Although the typhoon surges may lead to sediment resuspension in the study area (Li et al., 2015), the ^{210}Pb activity of core C10 shows no significant inversion over a multi-decadal timescale (Figure 2c), consistent with findings from previous studies (Gao et al., 2017, 2019). Therefore, we propose that cores C07 and C10 provide a relatively reliable chronological framework on a centennial or longer timescale.

4.2 Provenance of coarse fragments and their reliability as a typhoon indicator

The mineralogical composition (relative proportions of quartz, feldspar, and lithic fragments) of the 63–500 μm fractions in core C10 closely resembles that of fluvial sediment from the Minjiang River (Figure 2e and Figure S1). Sediment discharged by the Minjiang River typically deposits within the estuary during calm weather conditions (Wang et al., 2020). However, surges caused by extreme events can resuspend the nearshore sediment, subsequently

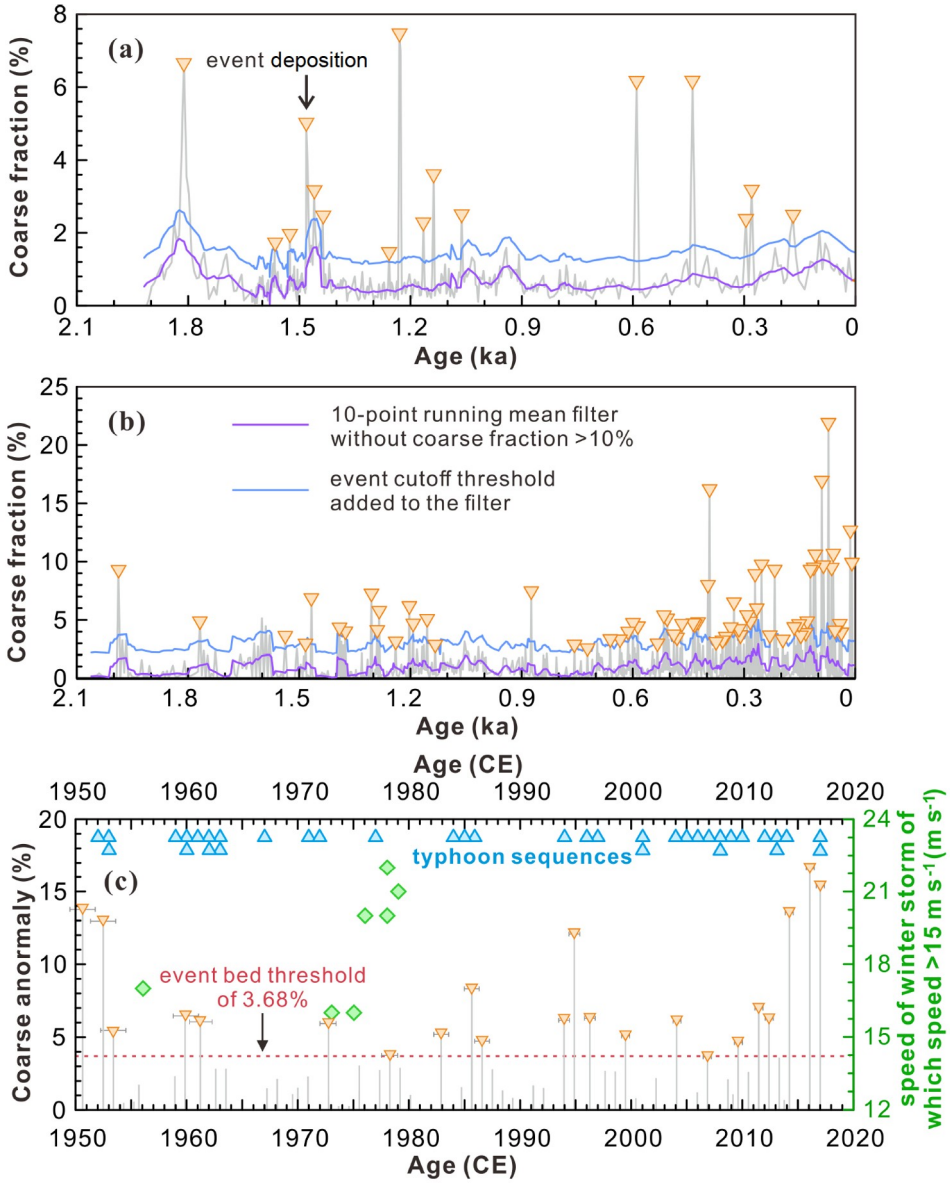

Figure 3 Typhoon events recorded in cores C07 and C10. Coarse fractions and typhoon event deposition in (a) core C07 and (b) core C10 before 1950 CE; (c) comparison between coarse anomaly in core C10, typhoon sequences, and speed of winter storms with wind speed >15 m s^{-1} during 1950 to 2020 CE.

generating offshore currents that transport coarse sediment to the muddy belt (Tian et al., 2019). Consequently, the coarse-grained sediment layers found in the muddy belt may serve as indicators of extreme events.

Earthquakes are frequent in Taiwan Island and the ocean to the east (Zhang, 2020). These seismic events contribute to the erosion of soil and bedrock, resulting in significant sediment discharge into the ocean (Dadson et al., 2005). Notably, nearly all fluvial sediment from Taiwan with a grain size >63 μm is deposited in nearshore areas (Milliman et al., 2007). The mineralogical composition of core C10 further suggests that coarse sediment from Taiwan is rarely transported across the strait (Figure 2e). Numerical simulations indicate that tsunamis have minimal impact on the East China Sea, primarily due to the damping of tsunami waves in shallow waters (Ren et al., 2013; Yang et al., 2017). While tsunamis originating from Japan or the South China Sea may exert some remote effects on the East China Sea, these influences are largely confined to sediment fractions <58 μm (Yang et al., 2017). Winter storms can also resuspend nearshore sediment, leading to offshore transport; however, the mean wind speeds associated with winter storms in the East China Sea typically range from 9 to 10 m s^{-1}, with only a few events exceeding 15 m s^{-1} (Dong et al., 2011; Figure 3c and Figure S2). In contrast, most typhoons produce wind speeds exceeding 25 m s^{-1} (Table S3). Thus, we propose that winter storms play a minor role in inducing surges and facilitating the offshore transport of coarse sediment.

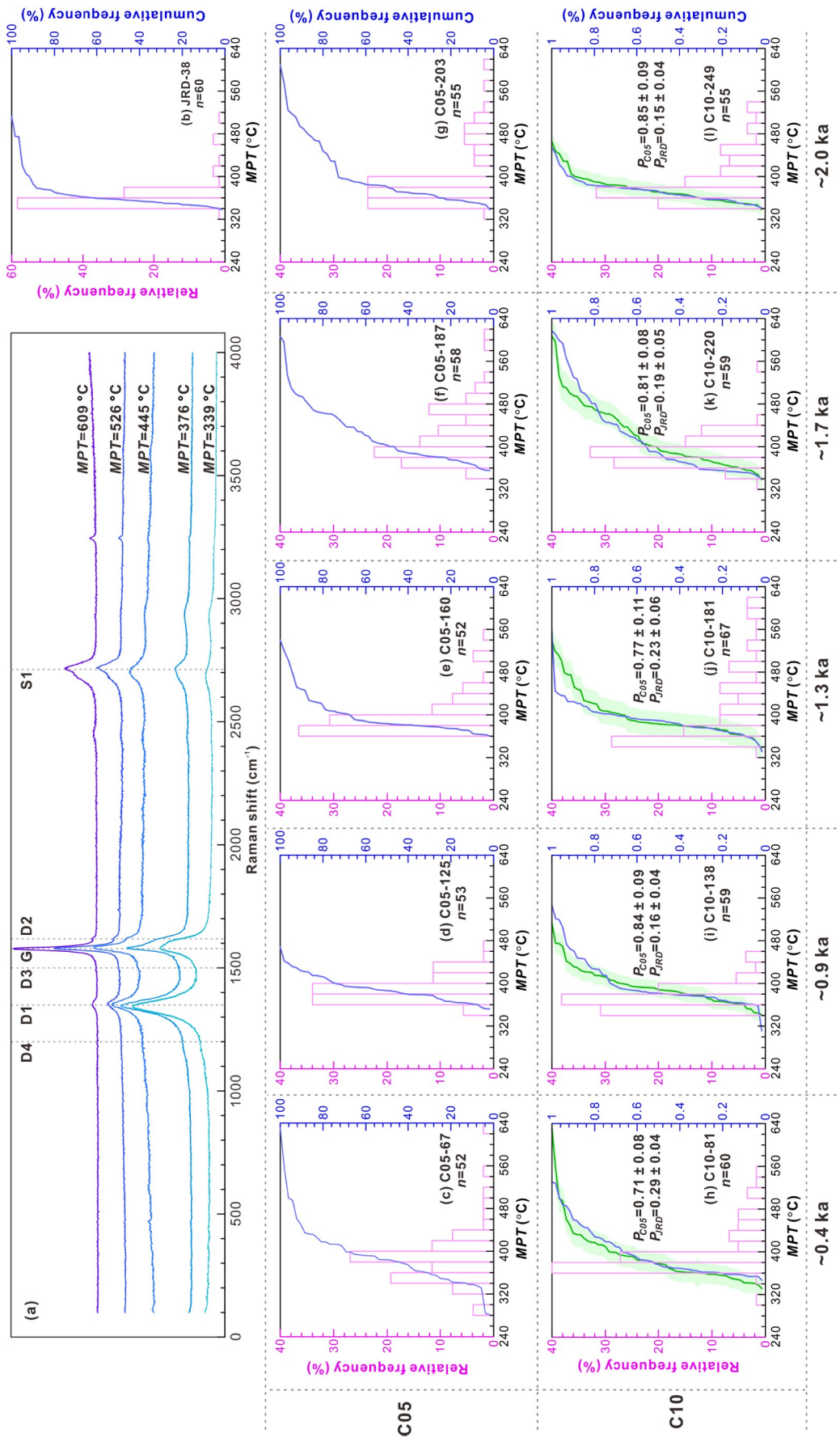

Figure 4 Raman spectral analysis of petrogenic organic carbon. (a) Raman spectra of organic carbon; distribution of MPT (b) JRD-38, (c–g) C05, and (h–l) C10. Observed probability and cumulative density functions are shown as pink histograms and blue curves, respectively. Predicted cumulative density functions in core C10 are shown as green curves.

Previous studies, based on numerical simulation and field investigation, have suggested that typhoons can increase the proportion of coarse fractions in the muddy belt (Li et al., 2015; Cong et al., 2023; Lin et al., 2024). Thus, it can be implied that the >63 μm fraction in the East China Sea muddy belt could be employed as a proxy for paleo-typhoon reconstruction (Zhou et al., 2019; Yang et al., 2022).

4.3 Reconstruction of paleo-typhoon frequency

To evaluate the sensitivity of samples to typhoon-induced deposition, we compared the event depositions, determined by the event threshold, at the top of core C10 with typhoon events in the study regions since 1950 CE (Figure 3c, Tables S3 and S4).

Within the age error margins, most event depositions in core C10 correspond to specific typhoon events (Figure 3c). This observation suggests that event depositions are a highly specific indicator of typhoons while remaining unaffected by other extreme events. However, not all typhoons resulted in event depositions that are preserved within the sedimentary record for core C10. The reasons for this are as follows: First, earlier event depositions may be disrupted by subsequent heavy typhoons, leading to the preservation of only the later event deposition in the sedimentary record, e.g., Typhoon Betty in 1972 CE (No. 197209, with a maximum wind speed of 50 m s^{-1} during its passage), which may destroy the event depositions formed by previous typhoons. Second, the thickness of the event layers formed by typhoons may be insufficient to withstand subsequent biological disturbance or physical alteration and compaction. Studies have indicated that event layers formed during typhoon passage must exceed 10 cm to be ultimately preserved in the sedimentary record (Lin et al., 2024). The factors determining the thickness of event layers are quite complex, including the strength, path, and duration of typhoons, as well as the distance from the sampling location. Third, the analytical resolution is 0.25 cm in the core C10, while the deposition rate, based on ^{210}Pb, at the top of the core is ~0.5 cm yr^{-1}. Given the heterogeneity of deposition rates, when multiple typhoons occur within a single year, the core C10 may not effectively capture the event depositions associated with each typhoon.

This study acknowledges the inherent uncertainty in the quantitative reconstruction of typhoon frequency from sedimentary records, primarily due to the preservation rates of typhoon-related depositions. This resulted in a probable underestimation of the historical frequency of typhoons in this study. However, the sedimentary environment of the East China Sea continental shelf has remained relatively stable over the past 2,000 yr (Zhang et al., 2022a), suggesting that significant changes in the factors influencing the preservation rates of event depositions are unlikely. Therefore, the trends in typhoon variability inferred from cores C10 and C07 are considered comparable.

Core C10 exhibited periods of frequent typhoons during ~1.6 to 1.1 ka and ~0.7 to 0 ka. Notably, during the LIA, the frequency of typhoons recorded in core C10 peaked, with >10 events per century (Figure 5d). Core C07 also exhibited high-frequency typhoon periods synchronous with core C10: ~1.6 to 1.0 ka and ~0.6 to 0 ka (Figure 5e). However, the number of reconstructed typhoon events in core C10 was twice more than that in core C07 during the LIA. Considering the distance between these two cores, the spatial difference in typhoon frequency may play a minor role in this discrepancy. A possible interpretation is that core C07 is not as sensitive as core C10, which could be due to two reasons. First, sand discharged from the Oujiang River is less likely to be transported to core C07 due to the island barrier. Second, compared to C10 (~25 m), C07 is situated at a greater depth (~40 m), implying that sandy sediments transported by offshore currents will be less abundant here. Consequently, the conditions for the formation of typhoon event depositions in core C07 are more stringent. Although the local environment results in differences in sensitivity between these two cores, the sedimentary environment of the muddy belt was stable during the last 2 millennia. This stability ensures that the typhoon frequency recorded in the two cores is comparable.

4.4 Proportion of fine sediment sourced from Taiwan

Silt and clay are scarce in the Minjiang River (Figure 2d), and mineralogy indicates that the 23~63 μm fractions in core C10 are contributed by Taiwan rivers and the Yangtze River (Figure 2f and Figure S3). Therefore, the provenance analysis of the fine fraction revealed two end-member sources for the provenance of C10: The Yangtze River and Taiwan, represented by samples from core C05 and JRD-N, respectively. Sediments from Taiwan showed relatively high proportions at ~0.4 and ~1.3 ka, with values of (29±4)% and (23±6)%, respectively. Their proportions declined at ~0.9, ~1.7, and ~2.0 ka, with values of (16±4)%, (19±5)%, and (15±4)%, respectively (Figure 5d). These results suggest that the influence of sediments from Taiwan on core C10 varied over time, with significant fluctuations during the late Holocene. The periods with higher proportions of sediment from Taiwan correspond to known periods of increased typhoon activity, indicating a potential link between typhoon intensity and the transport of fine sediments from Taiwan.

5. Discussions

Paleo-typhoon reconstruction in cores C07 and C10 indicates relatively frequent typhoon events in the southern East China Sea during the cooler climate periods of the last two mil-

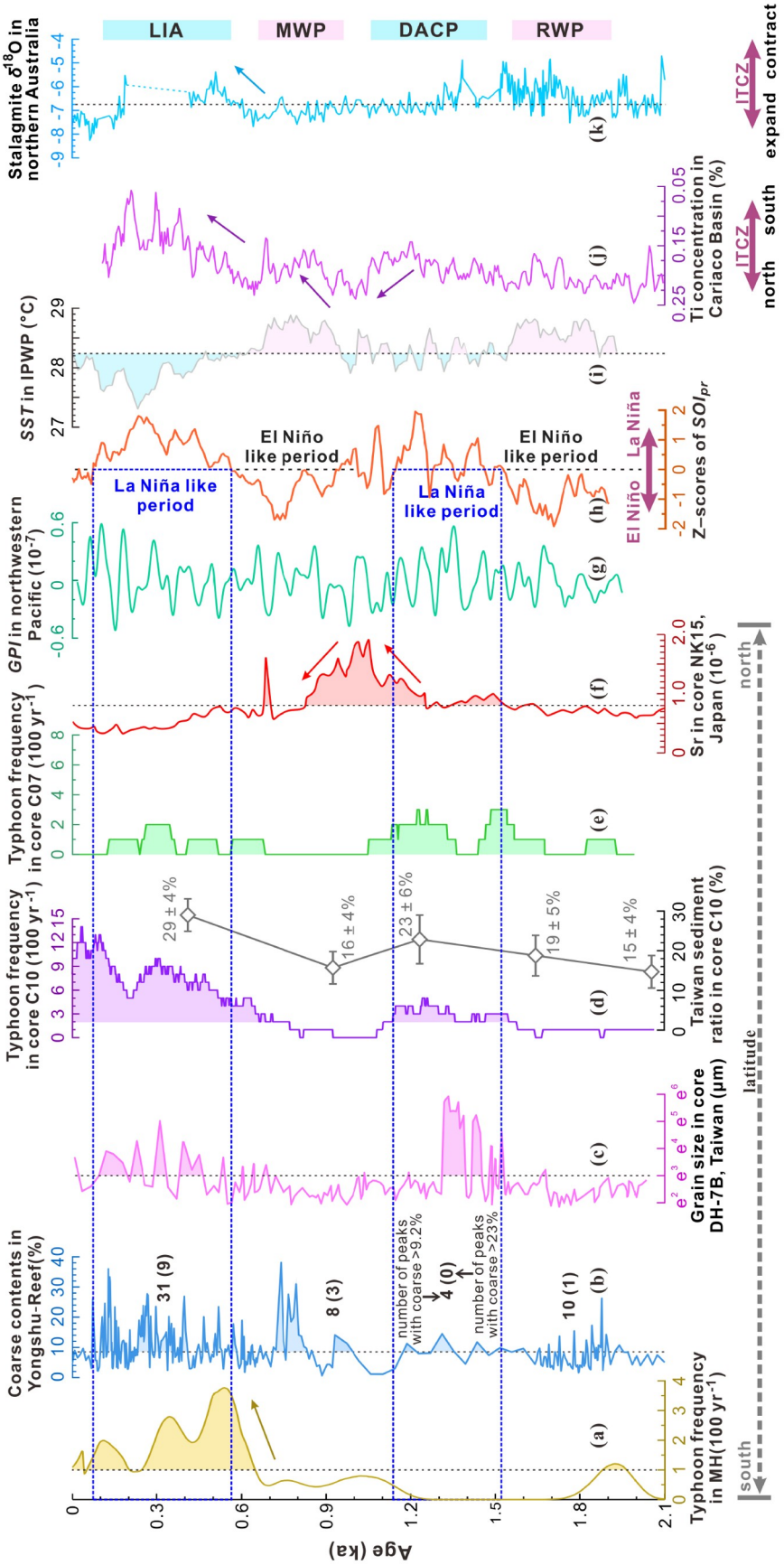

Figure 5 Comparison between paleo-typhoon reconstruction and paleoclimatic proxies in the northwestern Pacific. (a) Typhoon frequency in Marshall Islands (MH, Bramante et al., 2020); (b) coarse fraction of sediment in the Yongshu-Reef, South China Sea (Yu et al., 2009); (c) mean grain size in lacustrine sediment core DH-7B, Taiwan (Chen et al., 2012); (d) typhoon frequency (purple) and ratio of Taiwan-source sediment (gray) in core C10; (e) typhoon frequency in core C07; (f) Sr content of lacustrine sediment core NK15, Japan (Woodruff et al., 2009); (g) typhoon genesis potential index (GPI) in the northwestern Pacific (Yan et al., 2015); (h) Southern Oscillation Index (SOI_{pr}, Yan et al., 2011); (i) SST in the IPWP in cores BJ8 and MD60 (Oppo et al., 2009); (j) Ti concentration in sediment core in Cariaco Basin (Haug et al., 2001); (k) stalagmite $\delta^{18}O$ in KNI-51, northern Australia (Denniston et al., 2016). Samples' locations are shown in Figure 1. RWP: Roman Warm Period; DACP: Dark Age Cold Period; MWP: Medieval Warm Period; LIA: Little Ice Age.

lennia, i.e., the DACP and the LIA (Figure 5d and 5e). Concurrently, the fine fraction in core C10 showed a relatively high proportion of sediment from Taiwan, whose transport process is controlled by typhoons (Figure 5d). Meanwhile, paleo-typhoon reconstruction from cores ZM01 and T08 in the East China Sea muddy belt indicated that intensified typhoon periods were consistent with warm eras in the northern East China Sea (Zhou et al., 2019; Yang et al., 2022, Figure S4). In this study, the paleo-typhoon reconstruction was based on sand content, which is primarily influenced by typhoon frequency (Zhou et al., 2019). However, the paleo-typhoon proxies in cores ZM01 and T08 showed a positive correlation with typhoon intensity, based on comparisons of sediment records with decadal meteorological data (Zhou et al., 2019; Yang et al., 2022). The difference between this study and previous studies may be due to the asynchrony between periods of frequent and intensified typhoons.

To investigate the mechanism behind the oscillation of typhoon frequency recorded in cores C07 and C10, we compared the existing paleo-typhoon records and paleo-climatic reconstructions in the northwestern Pacific. The high grain size anomaly in lacustrine sediment in Taiwan, an indicator of typhoon-induced deposition, showed temporal consistency with frequent typhoon periods (Chen et al., 2012, Figure 5c). This indicates that typhoons were frequent during the DACP and LIA in southeast China. In the landfall regions of hurricanes in the northern Atlantic, their active periods may result from an increase in hurricanes in the ocean basin or the migration of dominant hurricane tracks (Donnelly and Woodruff, 2007; Wallace et al., 2019). Logically, the mechanism of typhoon activity in the northwestern Pacific is similar. The typhoon genesis potential index in the entire northwestern Pacific, reconstructed by the Community Earth System Model, showed no periodical change in the favorability of typhoon formation like the typhoon frequency along southeast China (Figure 5g, Yan et al., 2015). Additionally, most paleo-typhoon reconstructions in the northwestern Pacific were not synchronous with frequent typhoon activities in southeast China (Woodruff et al., 2009; Yu et al., 2009; Chen et al., 2012; Yue et al., 2019; Zhou et al., 2019; Bramante et al., 2020; Yang et al., 2022, Figures S4 and S5). Thus, the variation of typhoon frequency in the ocean basin could not explain its oscillation in southeast China over the past 2000 yr.

Paleo-typhoon events in Japan, located at a higher latitude in the northwestern Pacific, were prominent during the MWP, but quiescent during the DACP and LIA (Woodruff et al., 2009, Figure 5f). The seesaw-like typhoon activity between southeast China and Japan could be explained by the migration of typhoon tracks. Furthermore, the active typhoon periods in southeast China and Japan were consistent with La Niña-like and El Niño-like periods, respectively. Both the meteorological data and model results suggest that typhoons in the northwestern Pacific are closely associated with ENSO phases within years to decades. Elsner and Liu (2003) categorized the typhoons in this region into three distinct tracks: straight-moving, recurving, and north-oriented tracks (Figure 1b). During the La Niña years, the frequency of straight-moving typhoons, which primarily make landfall in southeast China, is significantly higher than that of recurving typhoons, which mainly affect Japan. Conversely, during the El Niño years, the frequency of straight-moving typhoons is markedly lower (Figure 1e). The simulation results also suggest that compared with the El Niño years, the typhoon genesis in the northwestern Pacific is more westward during the La Niña years (Gao and Zhou, 2022).

The genesis of typhoons requires the SST to be at least 26.5°C (Gray, 1968), making it an indispensable factor in the study of typhoons (Wu, 2024). Although the IPWP extends eastward during the El Niño years, the number of typhoons does not increase significantly due to the modulation of subsurface heat content changes in the tropical central-north Pacific (Gao et al., 2022, 2025). Consequently, the influence of ENSO on typhoons tends to induce variations in track patterns rather than altering their overall numbers. During the El Niño years, the IPWP expands and exhibits warm abnormal SST, leading to the eastward migration of the rising limb of the Walker Circulation (Thual and Dewitte, 2023) and the poleward expansion of the Hadley Cell (Sharmila and Walsh, 2018). This would cause migration of the location of typhoon genesis in the same direction (Bramante et al., 2020). Additionally, during the El Niño years, typhoon trajectories tend to recurve northward (Patricola et al., 2018), making typhoons more frequent in Japan. Conversely, the opposite hydrologic and atmospheric conditions of the Pacific during the La Niña years could contribute to the opposite migration of typhoon tracks. Over a multi-centennial timescale, during the La Niña-like periods, the relatively cooler IPWP (Oppo et al., 2009, Figure 5i) would cause the equatorward migration of typhoon genesis and tracks, resulting in more typhoons making landfall in southeast China (Figure 6). Based on the spatial distribution of sea SST anomalies in the tropical Pacific, El Niño events are classified into the eastern Pacific type and the central Pacific (CP) type. Furthermore, the CP type can be further divided into CP-I and CP-II (Wang and Wang, 2013, Figure S6). Research indicates that during these three types of El Niño events, the number of typhoons making landfall in Japan is higher than in normal years. In contrast, in southeast China, a significant increase in typhoon activity is observed only during CP-I El Niño periods (Pan et al., 2024). Consequently, we propose that El Niño has a more promotive impact on typhoon frequency in Japan, while the influence of CP-I El Niño on typhoon occurrences in southeast China should not be overlooked. It is necessary to reconstruct the paleo-SST with

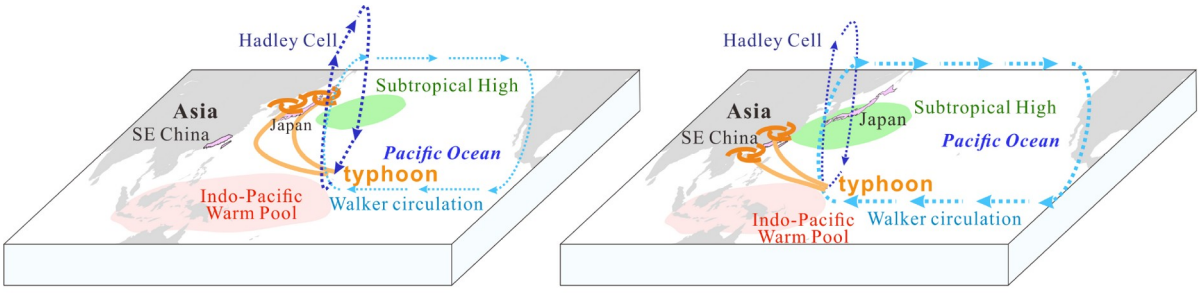

(a) El Niño-like period **(b) La Niña-like period**

Figure 6 Mechanism of typhoon routes migration in the northwestern Pacific over a multi-centennial timescale.

high temporal resolution in the tropical Pacific to identify different types of El Niño over a multi-centennial timescale and their influence on typhoon tracks in further studies. A recent study indicates that multi-year ENSO events were more frequent during the late Holocene (Lu et al., 2025). This phenomenon may reinforce the relationship between ENSO and typhoon tracks during the last 2 ka. Additionally, the South China Sea, another region of typhoon genesis (Figure 1a), showed low typhoon activity during pre-LIA, indicated by the grain size of lagoon sediment in the Yongshu Reef (Yu et al., 2009, Figure 5b). Therefore, the influence of typhoons from the South China Sea on southeast China could be minor at this stage.

During the LIA, typhoons were remarkably frequent in the South China Sea and the Marshall Islands, which are at lower latitudes than southeast China, compared to those in pre-LIA (Figure 5a and 5b). Notably, the ITCZ in the Pacific migrated southward and contracted during the LIA (Haug et al., 2001; Denniston et al., 2016, Figure 5j and 5k). Approximately 70% of typhoons are generated in the ITCZ (Studholme et al., 2022), implying that the typhoon genesis migrated southward during the LIA. Typhoons generated in the South China Sea were more frequent and may influence southeast China. Thus, the peak maximum typhoon frequency in southeast China was a consequence of the coupling between La Niña-like conditions and the contraction and migration of the ITCZ.

ENSO events are known to play key roles in the global climate on different timescales. The ENSO events were more frequent and complex during the late Holocene (Moy et al., 2002; Lu et al., 2025), and this study emphasized the influence of ENSO phases on typhoon tracks over a multi-centennial timescale. Additionally, both coarse and fine fractions were analyzed for paleo-typhoon reconstruction based on provenance investigation. We demonstrated that in specific environments, typhoon activities could also be revealed by fine sediment, which has been ignored in previous studies. These findings provide new insights for paleoclimatic, paleoenvironmental, and sedimentological research.

6. Conclusions

This study quantified paleo-typhoon frequency based on coarse sediment analysis and investigated the proportion of typhoon-induced fine sediment in southeast China over the last 2000 yr. Two active typhoon periods, i.e., ~1.6 to 1.1 ka and ~0.7 to 0 ka, coincided with La Niña-dominated intervals, highlighting the critical role of ENSO phases in the migration of typhoon tracks. During the La Niña-like periods, the cooler IPWP induced a southwestward migration of typhoons by driving the migration of the Walker Circulation and Hadley Cell, causing frequent typhoons in southeast China. The peak maximum typhoon frequency in southeast China during the LIA was a consequence of the combined effects of La Niña-like conditions and the contraction and migration of the ITCZ. Meanwhile, the Taiwan-sourced sediment exhibited relatively high proportions in the East China Sea muddy belt, indicating the contribution of frequent typhoons to the deposition of Taiwan-sourced sediment over a multi-centennial timescale. Our findings are expected to be significant for paleoclimate, paleoenvironment, and sedimentology studies in East Asia, providing a new perspective and basis for understanding the relationship between typhoon activities and climate change.

Acknowledgements *We thank Qiang LIU, Qiao AI, and Youshan XU for their help with fieldwork, and Qiaozhi LI, and Ye QIU for their help with lab analysis. We appreciate Prof. Robert Sparkes' suggestions on the Raman analysis. We are grateful to two anonymous reviewers for their thoughtful reviews that improved this manuscript. This study was supported by the National Key Research and Development Program of China (Grant No. 2023YFF0804701), the National Natural Science Foundation of China (Grant Nos. 42276170, 41776048 and 42106158), and the Fundamental Research Funds for the Central Universities (Grant No. 020914380142). The new data in this study were updated in the supplement materials, including the supporting information and dataset, and they were also uploaded to the Open Science Framework (https://osf.io/m7r5z/). The typhoon tracks were referenced from "Best Track Dataset for Tropical Cyclones over the western North Pacific", which was obtained from www.typhoon.gov.cn, the meteorological data was obtained from www.ncei.noaa.gov.*

Conflict of interest The authors declare no conflict of interest.

Supporting information The supporting information is available online at http://earth.scichina.com and http://link.springer.com. The supporting materials are published as submitted, without typesetting or editing. The responsibility for scientific accuracy and content remains entirely with the authors.

References

Beyssac O, Goffé B, Chopin C, Rouzaud J N. 2002. Raman spectra of carbonaceous material in metasediments: A new geothermometer. J Metamorph Geol, 20: 859–871

Blaauw M, Christen J A. 2011. Flexible paleoclimate age-depth models using an autoregressive gamma process. Bayesian Anal, 6: 457–474

Bramante J F, Ford M R, Kench P S, Ashton A D, Toomey M R, Sullivan R M, Karnauskas K B, Ummenhofer C C, Donnelly J P. 2020. Increased typhoon activity in the Pacific deep tropics driven by Little Ice Age circulation changes. Nat Geosci, 13: 806–811

Camargo S J, Robertson A W, Gaffney S J, Smyth P, Ghil M. 2007. Cluster analysis of typhoon tracks. Part II: Large-scale circulation and ENSO. J Clim, 20: 3654–3676

Chan J C L. 2006. Comment on "Changes in tropical cyclone number, duration, and intensity in a warming environment". Science, 311: 1713

Chen H, Wen S, Song S, Yang T, Lee T, Lin S, Hsu S, Wei K, Chang P, Yu P. 2012. Strengthening of paleo-typhoon and autumn rainfall in Taiwan corresponding to the Southern Oscillation at late Holocene. J Quat Sci, 27: 964–972

Cong S, Wu X, Ge J, Bi N, Li Y, Lu J, Wang H. 2023. Intermittent migration of mixing front driven by typhoon events on the inner shelf of the East China Sea: A FVCOM modeling study. Mar Geol, 465: 107161

Dadson S, Hovius N, Pegg S, Dade W B, Horng M J, Chen H. 2005. Hyperpycnal river flows from an active mountain belt. J Geophys Res, 110: 2004JF000244

Denniston R F, Ummenhofer C C, Wanamaker A D, Lachniet M S, Villarini G, Asmerom Y, Polyak V J, Passaro K J, Cugley J, Woods D, Humphreys W F. 2016. Expansion and contraction of the Indo-Pacific tropical rain belt over the last three millennia. Sci Rep, 6: 34485

Dong L X, Guan W B, Chen Q, Li X H, Liu X H, Zeng X M. 2011. Sediment transport in the Yellow Sea and East China Sea. Estuar Coast Shelf Sci, 93: 248–258

Donnelly J P, Woodruff J D. 2007. Intense hurricane activity over the past 5,000 years controlled by El Niño and the West African monsoon. Nature, 447: 465–468

Donnelly J P, Hawkes A D, Lane P, MacDonald D, Shuman B N, Toomey M R, van Hengstum P J, Woodruff J D. 2015. Climate forcing of unprecedented intense-hurricane activity in the last 2000 years. Earths Future, 3: 49–65

Elsner J B, Liu K. 2003. Examining the ENSO-typhoon hypothesis. Clim Res, 25: 43–54

Emanuel K. 2005. Increasing destructiveness of tropical cyclones over the past 30 years. Nature, 436: 686–688

Gao C, Zhou L. 2022. Tropical cyclone genesis over the western North Pacific simulated by Coupled Model Intercomparison Project Phase 6 models. Acta Oceanol Sin, 41: 64–77

Gao C, Zhou L, Wang C, Lin I I, Murtugudde R. 2022. Unexpected limitation of tropical cyclone genesis by subsurface tropical central-north Pacific during El Niño. Nat Commun, 13: 7746

Gao C, Zhou L, Lin I I, Wang C, Guan S, Jin F F, Murtugudde R. 2025. Crucial role of subsurface ocean variability in tropical cyclone genesis. Nat Commun, 16: 1050

Gao J H, Jia J, Sheng H, Yu R, Li G C, Wang Y P, Yang Y, Zhao Y, Li J, Bai F, Xie W, Wang A, Zou X, Gao S. 2017. Variations in the transport, distribution, and budget of ^{210}Pb in sediment over the estuarine and inner shelf areas of the East China Sea due to Changjiang catchment changes. J Geophys Res-Earth Surf, 122: 235–247

Gao J H, Shi Y, Sheng H, Kettner A J, Yang Y, Jia J J, Wang Y P, Li J, Chen Y, Zou X, Gao S. 2019. Rapid response of the Changjiang (Yangtze) River and East China Sea source-to-sink conveying system to human induced catchment perturbations. Mar Geol, 414: 1–17

Goldburg E D, Koide M. 1963. Rates of sediment accumulation in the Indian Ocean. In: Geiss J, Goldberg E D, eds. Earth Science and Meteoritics. Amsterdam: North-Holland Publishing Company. 90–102

Goldenberg S B, Landsea C W, Mestas-Nunez A M, Gray W M. 2001. The recent increase in Atlantic Hurricane activity: Causes and implications. Science, 293: 474–479

Gray W M. 1968. Global view of the origin of tropical disturbances and storms. Mon Weather Rev, 96: 669–700

Haug G H, Hughen K A, Sigman D M, Peterson L C, Rohl U. 2001. Southward migration of the intertropical convergence zone through the Holocene. Science, 293: 1304–1308

Jian X, Zhang W, Yang S, Kao S. 2020. Climate-dependent sediment composition and transport of mountainous rivers in tectonically stable, Subtropical East Asia. Geophys Res Lett, 47: e2019GL086150

Jiao R, Herman F, Beyssac O, Adatte T, Cox S C, Nelson F E, Neil H L. 2018. Erosion of the Southern Alps of New Zealand during the last deglaciation. Geology, 46: 975–978

Lane P, Donnelly J P, Woodruff J D, Hawkes A D. 2011. A decadally-resolved paleohurricane record archived in the late Holocene sediments of a Florida sinkhole. Mar Geol, 287: 14–30

Lahfid A, Beyssac O, Deville E, Negro F, Chopin C, Goffé B. 2010. Evolution of the Raman spectrum of carbonaceous material in low-grade metasediments of the Glarus Alps (Switzerland). Terra Nova, 22: 354–360

Li Y, Li H, Qiao L, Xu Y, Yin X, He J. 2015. Storm deposition layer on the Fujian coast generated by Typhoon Saola (2012). Sci Rep, 5: 14904

Li Y, Xu X, Zheng B. 2018. Satellite views of cross-strait sediment transport in the Taiwan Strait driven by Typhoon Morakot (2009). Cont Shelf Res, 166: 54–64

Lin Y, Li Y, Liu M, Wang L, Zheng B, Long Z, Xu J. 2024. Typhoon Chan-Hom (2015) induced sediment cross-shore transport in the mud depocenter of the East China Sea inner shelf. Mar Geol, 469: 107223

Liu X, Li A, Dong J, Lu J, Huang J, Wan S. 2018. Provenance discrimination of sediments in the Zhejiang-Fujian mud belt, East China Sea: Implications for the development of the mud depocenter. J Asian Earth Sci, 151: 1–15

Lu Z, Schultze A, Carré M, Brierley C, Hopcroft P O, Zhao D, Zheng M, Braconnot P, Yin Q, Jungclaus J H, Shi X, Yang H, Zhang Q. 2025. Increased frequency of multi-year El Niño-Southern Oscillation events across the Holocene. Nat Geosci, 18: 337–343

Mei W, Xie S P, Primeau F, McWilliams J C, Pasquero C. 2015. Northwestern Pacific typhoon intensity controlled by changes in ocean temperatures. Sci Adv, 1: e1500014

Milliman J D, Lin S W, Kao S J, Liu J P, Liu C S, Chiu J K, Lin Y C. 2007. Short-term changes in seafloor character due to flood-derived hyperpycnal discharge: Typhoon Mindulle, Taiwan, July 2004. Geology, 35: 779–782

Moy C M, Seltzer G O, Rodbell D T, Anderson D M. 2002. Variability of El Niño/Southern Oscillation activity at millennial timescales during the Holocene epoch. Nature, 420: 162–165

Oppo D W, Rosenthal Y, Linsley B K. 2009. 2,000-year-long temperature and hydrology reconstructions from the Indo-Pacific warm pool. Nature, 460: 1113–1116

Pan L, Wang X, Chen J, Zhan H. 2024. Distinct features of tropical cyclone landfall over East Asia during various types of El Niño. J Clim, 37: 4989–5008

Patricola C M, Camargo S J, Klotzbach P J, Saravanan R, Chang P. 2018. The influence of ENSO flavors on western North Pacific tropical cyclone activity. J Clim, 31: 5395–5416

Ren Z, Wang B, Fan T, Liu H. 2013. Numerical analysis of impacts of 2011 Japan Tohoku tsunami on China Coast. J Hydrodyn, 25: 580–590

Sharmila S, Walsh K J E. 2018. Recent poleward shift of tropical cyclone formation linked to Hadley cell expansion. Nat Clim Change, 8: 730–736

Sobel A H, Camargo S J, Hall T M, Lee C Y, Tippett M K, Wing A A.

2016. Human influence on tropical cyclone intensity. Science, 353: 242–246
Sparkes R B, Hovius N, Galy A, Liu J T. 2020. Survival of graphitized petrogenic organic carbon through multiple erosional cycles. Earth Planet Sci Lett, 531: 115992
Studholme J, Fedorov A V, Gulev S K, Emanuel K, Hodges K. 2022. Poleward expansion of tropical cyclone latitudes in warming climates. Nat Geosci, 15: 14–28
Thual S, Dewitte B. 2023. ENSO complexity controlled by zonal shifts in the Walker circulation. Nat Geosci, 16: 328–332
Tian Y, Fan D, Zhang X, Chen B, Wang L, Liu M, Yang Z. 2019. Event deposits of intense typhoons in the muddy wedge of the East China Sea over the past 150 years. Mar Geol, 410: 109–121
Wallace E J, Donnelly J P, van Hengstum P J, Wiman C, Sullivan R M, Winkler T S, d'Entremont N E, Toomey M, Albury N. 2019. Intense hurricane activity over the past 1500 years at South Andros Island, The Bahamas. Paleoceanogr Paleocl, 34: 1761–1783
Wang A, Ye X, Lin Z. 2020. Sediment transport in a mountainous river subaquesous delta and its response to marine sand extraction: A cast study of Minjiang River Estuary, Southeast China Coast. In: Proceedings of the 10th International Conference on Asian and Pacific Coasts. Hanoi. 725–729
Wang B, Chan J C L. 2002. How strong ENSO events affect tropical storm activity over the western North Pacific. J Clim, 15: 1643–1658
Wang C, Wang X. 2013. Classifying El Niño Modoki I and II by different impacts on rainfall in southern China and typhoon tracks. J Clim, 26: 1322–1338
Webster P J, Holland G J, Curry J A, Chang H R. 2005. Changes in tropical cyclone number, duration, and intensity in a warming environment. Science, 309: 1844–1846
Woodruff J D, Donnelly J P, Okusu A. 2009. Exploring typhoon variability over the mid-to-late Holocene: Evidence of extreme coastal flooding from Kamikoshiki, Japan. Quat Sci Rev, 28: 1774–1785
Wu L. 2024. New findings on the influence of El Niño events on tropical cyclone formation. Sci China Earth Sci, 67: 892–893
Yan H, Sun L, Wang Y, Huang W, Qiu S, Yang C. 2011. A record of the Southern Oscillation Index for the past 2,000 years from precipitation proxies. Nat Geosci, 4: 611–614
Yan Q, Korty R, Zhang Z. 2015. Tropical cyclone genesis factors in a simulation of the last two millennia: Results from the community earth system model. J Clim, 28: 7182–7202
Yang W, Zhou X, Xiang R, Wang Y, Sun L. 2017. Palaeotsunami in the East China Sea for the past two millennia: A perspective from the sedimentary characteristics of mud deposit on the continental shelf. Quat Int, 452: 54–64
Yang Y, Zhou L, Normandeau A, Jia J, Yin Q, Wang Y P, Shi B, Gao L, Gao S. 2020a. Exploring records of typhoon variability in eastern China over the past 2000 years. GSA Bull, 132: 2243–2252
Yang Y, Maselli V, Normandeau A, Piper D J W, Li M Z, Campbell D C, Gregory T, Gao S. 2020b. Latitudinal response of storm activity to abrupt climate change during the last 6,500 years. Geophys Res Lett, 47: e2020GL089859
Yang Y, Piper D J W, Xu M, Gao J, Jia J, Normandeau A, Chu D, Zhou L, Wang Y P, Gao S. 2022. Northwestern Pacific tropical cyclone activity enhanced by increased Asian dust emissions during the Little Ice Age. Nat Commun, 13: 1712
Yu K F, Zhao J X, Shi Q, Meng Q S. 2009. Reconstruction of storm/tsunami records over the last 4000 years using transported coral blocks and lagoon sediments in the southern South China Sea. Quat Int, 195: 128–137
Yue Y, Yu K, Tao S, Zhang H, Liu G, Wang N, Jiang W, Fan T, Lin W, Wang Y. 2019. 3500-year western Pacific storm record warns of additional storm activity in a warming warm pool. Palaeogeogr Palaeoclimatol Palaeoecol, 521: 57–71
Zhang S. 2020. Climate-driven provenance variation and drainage evolution of small mountainous rivers in Taiwan since the last ice age. Master Dissertation. Xiamen: Xiamen University
Zhang S, Liu S, Shu Z, Xu X, Lv J, Shi Y, Gao J. 2022a. Climate-driven provenance variation and sedimentary system evolution at the Changjiang distal mud since the mid-Holocene. Mar Geol, 452: 106902
Zhang S, Jian X, Liu J T, Wang P, Chang Y P, Zhang W. 2022b. Climate-driven drainage reorganization of small mountainous rivers in Taiwan (East Asia) since the last glaciation: The Zhuoshui River example. Palaeogeogr Palaeoclimatol Palaeoecol, 586: 110759
Zhang S, Liu S, Xu X, Lyu J, Zha B, Yang G, Liu T, Shi Y, Yang Y, Gao J. 2023. Marine ecological effect of typhoon influenced by the frequency-phases of ENSO and anthropogenic activity: The East China Sea example. Palaeogeogr Palaeoclimatol Palaeoecol, 629: 111783
Zhou X, Liu Z, Yan Q, Zhang X, Yi L, Yang W, Xiang R, He Y, Hu B, Liu Y, Shen Y. 2019. Enhanced tropical cyclone intensity in the western North Pacific during warm periods over the last two millennia. Geophys Res Lett, 46: 9145–9153

(Editorial handling: Zhongshi ZHANG)